HIGH WAVENUMBER CONVECTION IN TALL POROUS CONTAINERS HEATED FROM BELOW

By SAMANTHA LEWIS, D. A. S. REES

(*School of Mechanical Engineering, University of Bath, Claverton Down, Bath* BA2 7AY)

and ANDREW P. BASSOM

(*Department of Mathematics, University of Exeter, North Park Road, Exeter, Devon* EX4 4QE)

[Received 16 April 1996. Revise 20 January 1997]

SUMMARY

In this paper we consider convection in a high-aspect-ratio porous container which is heated from below and whose sidewalls are insulated. This paper presents asymptotic analyses of weakly nonlinear and highly nonlinear convection in the limit of large wavenumber, a. When a is $O(1)$, strongly nonlinear convection must be analysed using fully numerical methods, though, when a is large, some progress can be made using asymptotic methods without recourse to a direct simulation of the full governing equations.

The onset of convection is given by the usual linear stability analysis for the Darcy–Bénard problem, and the critical Rayleigh number is given by $R_c \sim a^2$ at leading order. As the Rayleigh number increases there are three nonlinear asymptotic regimes which may be considered, the first of which yields the familiar weakly nonlinear flow. In this regime, for which $R - R_c$ is asymptotically small, the weakly nonlinear evolution is given by the solution of a cubic Landau equation for the amplitude. When $R - R_c = O(1)$, the second regime, the flow is characterized by the fact that the mean correction to the temperature profile and the first harmonic appear at the same order in the asymptotic expansion. The amplitude of convection is now found to be given by an integro-differential equation and numerical solutions indicate that when $R - R_c$ is large boundary layers develop at the top and the bottom of the container.

The final regime emerges when R is so large that it is of size $R_c + O(a)$. The flow then separates into three distinct domains: two boundary layers form, one at either end of the container, and a core flow exists in the interior. These flows are given by a singular perturbation analysis and the equations describing the boundary layer flow constitute a nonlinear eigenvalue problem which requires numerical solution.

1. Introduction

THE SUBJECT of thermal convection in porous media has been studied extensively in recent years and the growing volume of work devoted to this and other topics in porous medium convection has been documented in the reviews by Tien and Vafai (1) and Nield and Bejan (2). There are many important reasons for the development of this subject. On the practical side, the need to model geothermal systems, packed-bed catalytic reactors and

heat storage beds continues to motivate further research towards a better understanding of transport phenomena in porous media. On the other hand, there is also a need to comprehend fully the implications of recent models of fluid flows within a porous matrix. An example of the latter is the recent paper of Rees (**3**) which details how the presence of inertia modifies stability boundaries in the Darcy–Bénard problem and hence determines the ranges of heat transfer rates which might be found in practice.

The motivation for the present work is the desire to understand the mechanisms which may drive nonlinear thermal convection in porous media flow in a long, thin rectangular container. We demonstrate below that highly nonlinear modes can be obtained using formal asymptotic methods as long as the Rayleigh number is not too large. In a typical weakly nonlinear analysis (see Stuart (**4**) or Watson (**5**)) a small-amplitude disturbance in the form of a cellular motion is imposed on the basic flow. If this amplitude is of size $O(\varepsilon)$, say, then the interaction of the cell with itself forces a second harmonic and a mean state correction both of size $O(\varepsilon^2)$. These in turn drive an $O(\varepsilon^3)$ correction to the fundamental component of the mode. A solvability (or orthogonality) criterion applied to the $O(\varepsilon^3)$ equations yields an equation for the scaled amplitude of the original disturbance. This type of analysis has been applied to a wide variety of situations but Palm *et al.* (**6**) were the first authors to apply the technique to porous medium convection in a layer heated from below.

This weakly nonlinear approach remains valid only if the amplitude of the convection cell is asymptotically small, and the deviation of the Rayleigh number from its critical value is $O(\varepsilon^2)$. One significant feature of this methodology is that the correction to the mean state induced by the interaction of the fundamental component with itself is asymptotically smaller than the original basic flow. But when the amplitude of the disturbance becomes too large, such as would be the case when R is too far above critical, then this is no longer true. Instead, the mean state is then altered by the convective motions and the mathematical nature of the problem is changed dramatically. In most stability problems whenever the leading order mean flow and the highly nonlinear disturbance are inextricably linked in this way then analytical progress is virtually impossible and one has to resort to a numerical solution of the full governing equations. However, recently it has been shown that this scenario does not occur in all cases. The first demonstration of an alternative was presented by Hall and Lakin (**7**) who studied nonlinear small wavelength Görtler vortices which can evolve in an isothermal boundary layer above a suitably concave plate. Such modes can be described by an asymptotic flow structure which shows that the vortices are confined to a well-defined region within the boundary layer. The vortices are sufficiently large so as to interact and drive a correction to the mean boundary layer profile which is of size comparable with the magnitude of the basic flow that would exist in the absence of vortices.

The overall mean flow is totally changed by the vortex modes and, in turn, the resulting form of the mean flow dictates the quantitative details of the vortex structure. Thus the mean flow–vortex interaction is fully coupled but, rather than necessitating a computational solution of the full Navier–Stokes equations, the problem is amenable to analytical treatment. In this case the problem is reduced to one in which the solution of a single free-boundary problem yields the location of the edges of the main activity zone of the vortex as the boundary layer evolves downstream.

The essential key for the analytical description of the nonlinear Görtler modes is the observation that a marked disparity exists between the two principal lengthscales involved; the spanwise vortex wavelength is much shorter than the characteristic distance over which the the boundary layer develops. Similar features have been subsequently exploited in order to derive strongly nonlinear modes in a number of other situations; by 'strongly nonlinear' here we mean vortex amplitudes which are far larger than the limit of the validity of standard weakly nonlinear theories. Blennerhassett and Bassom (**8**) illustrated that steady, highly nonlinear rolls are mathematically acceptable solutions of the classical Bénard convection problem. Their results were extended by Bassom and Zhang (**9**) who investigated nonlinear convection rolls in a rapidly rotating fluid layer. Such modes are believed to be important in a variety of geophysical applications and it was demonstrated how strongly nonlinear cells can affect significantly the characteristics of the flow and lead to greatly enhanced rates of heat transfer.

In the present article we apply the same asymptotic strongly nonlinear vortex theory to the problem of convection cells generated in a saturated porous medium which is confined within a large aspect ratio, tall container. The fact that the flow domain has a large aspect ratio makes the development of an appropriate strongly nonlinear theory possible. We restrict our attention to two-dimensional flows—this is a reasonable assumption for if the height of the (cuboidal) cavity is substantially greater than either its depth or its breadth, then the onset problem yields two-dimensional flow aligned such that fluid motion takes place in planes parallel with the vertical sides of greatest width. It is possible that three-dimensionality could arise if the horizontal cross-section is nearly square, and therefore we assume that the cross-section has a sufficiently large aspect ratio to preclude this. Given that modes in such a tall cavity are identical to those of the same wavelength in a horizontally unbounded layer (though presumably highly unstable in the latter case) our present work has more physical realism than those cases treated in (**8**) or (**9**), and is, indeed, fully realistic subject to the above geometrical constraint and the assumed absence of time-dependent instabilities.

The three increasingly nonlinear regimes we describe here can best be established sequentially by taking appropriate limits of the results arising from each regime and thereby inferring the scalings for the next. Indeed, the

details of the structure governing strongly nonlinear modes are sensitively dependent on the particular problem being considered. For example, the Görtler vortex work of Hall and Lakin (7) shows that the mode occupies a well-defined zone contained well within the boundary layer, whilst the theory of (8) shows that nonlinear modes in a Bénard layer fill the whole gap between the bounding horizontal surfaces. Thus it is not easy to anticipate the appropriate strongly nonlinear structure and this is best deduced via a gradual increase in vortex amplitude starting from the familiar weakly nonlinear case.

In view of this fact, the remainder of the paper proceeds as follows. In the next section we formulate the governing equations and review briefly the results of a standard weakly nonlinear analysis. As the vortex strength is increased a new stage of convection is reached in which the disturbance structure throughout the container is significantly altered. We call this state 'intermediate strength convection' for we then examine one further limit in which fully nonlinear boundary layers are set up at the top and bottom of the container. A simple eigenvalue problem can be obtained for intermediate strength convection and this is formulated and solved in section 3. The strongly nonlinear analysis is discussed in section 4 and we draw some conclusions in section 5.

2. Equations of motion and weakly nonlinear solutions

Consider the problem of free convection in an infinite layer of saturated porous medium bounded by two horizontal impermeable surfaces a distance d apart. The temperatures of the upper and lower surfaces bounding the medium are taken to be uniform and equal to T_u and T_l, respectively, with $T_l > T_u$. Cartesian coordinates (x, y, z) are oriented such that the y-axis is normal to the bounding surfaces of the fluid and gravity acts in the negative y-direction. The fluid is assumed to be such that Darcy's law holds and the Oberbeck–Boussinesq approximation is valid. The coefficient of thermal expansion, α, the thermal diffusivity, κ, and the viscosity, μ, are therefore all taken to be independent of the temperature T, whilst the density, ρ, depends linearly on variations in T. A scaled temperature θ is defined according to $T = T_u + \theta(T_l - T_u)$ and thence $\rho = \rho_u[1 - \alpha(T_l - T_u)\theta]$ where $\alpha(T_l - T_u)$ is assumed small. The resulting dimensionless Darcy–Boussinesq equations are

$$u_x + v_y = 0, \tag{2.1a}$$

$$u = -p_x, \tag{2.1b}$$

$$v = -p_y + R\theta, \tag{2.1c}$$

$$u\theta_x + v\theta_y = \theta_{xx} + \theta_{yy}, \tag{2.1d}$$

if steady two-dimensional velocity fields are considered. Here R denotes the Darcy–Rayleigh number of the flow

$$R = \frac{g\alpha K d(T_l - T_u)}{\mu\kappa} \tag{2.1e}$$

and the specification of the problem is completed by the boundary conditions

$$v = 0, \qquad \theta = 1 - y \qquad \text{on} \qquad y = 0 \quad \text{and} \quad y = 1. \tag{2.2}$$

It is well known that the conduction state $\theta = 1 - y$, $u = v = 0$ is unstable to small temperature perturbations proportional to $\cos ax$, say, when the Darcy–Rayleigh number is sufficiently high, and, in particular, there is a neutral stability curve $R = R_N(a)$ relating R and the wavenumber, a, at the onset of convection. When $R > R_N(a)$ then small-amplitude disturbances grow in time, but if $\varepsilon^2 = R - R_N(a) > 0$ is small then a nonlinear analysis shows that equilibrium solutions with $O(\varepsilon)$ amplitude are possible; see Palm, Weber and Kvernvold (**6**) and Rees and Riley (**10, 11**). A full stability analysis of weakly nonlinear solutions in a layer of infinite horizontal extent may be gleaned from (**10, 11**), but as the present paper is ultimately concerned with convection in a large-aspect ratio container we shall not dwell on their results here.

For the purpose of the weakly nonlinear analysis of the basic conduction state we introduce a streamfunction $\psi(x, y)$ such that

$$u = -\psi_y, \qquad v = \psi_x,$$

so that the governing equations (2.1a to d) may be recast as

$$\nabla^2\psi = R\theta_x, \tag{2.3a}$$

$$\psi_x\theta_y - \psi_y\theta_x = \nabla^2\theta, \tag{2.3b}$$

subject to the boundary conditions

$$\psi = 0, \quad \theta = 1 \quad \text{on} \quad y = 0 \qquad \text{and} \qquad \psi = 0, \quad \theta = 0 \quad \text{on} \quad y = 1. \tag{2.3c}$$

In (2.3b), ∇^2 denotes the two-dimensional Laplacian operator in the (x, y)-plane.

For Darcy–Rayleigh numbers close to the neutral value $R_N(a)$ the standard weakly nonlinear analysis for vortices of wavenumber a starts with expansions

$$\psi = \varepsilon A\phi_{11}(y)\sin ax + \varepsilon^2 A^2\phi_{22}(y)\sin 2ax + \varepsilon^3 A^3\left[\phi_{31}(y)\sin ax + \phi_{33}(y)\sin 3ax\right] + \ldots, \tag{2.4a}$$

$$\theta = 1 - y + \varepsilon AT_{11}(y)\cos ax + \varepsilon^2 A^2\left[T_{20}(y) + T_{22}(y)\cos 2ax\right] + \varepsilon^3 A^3\left[T_{31}(y)\cos ax + T_{33}(y)\cos 3ax\right] + \ldots, \tag{2.4b}$$

$$R = R_N + \varepsilon^2 R_2 + \ldots, \tag{2.4c}$$

where $R_2 = O(1)$ as $\varepsilon \to 0$. The equations for the ϕ_{ij} and T_{ij} terms form pairs of second order coupled linear equations which must be solved sequentially. The leading order equations for ϕ_{11} and T_{11} constitute a linear eigenvalue problem for R_N whose solution is

$$R_N = \frac{(\pi^2 + a^2)^2}{a^2}, \qquad T_{11} = \sin \pi y, \qquad \phi_{11} = \frac{(\pi^2 + a^2)}{a} \sin \pi y. \quad (2.5a, b, c)$$

At second order in ε we obtain

$$\phi_{22} = 0, \qquad T_{22} = 0, \qquad T_{20} = -\frac{(\pi^2 + a^2)}{8\pi} \sin 2\pi y \qquad (2.5d, e, f)$$

whilst the equations for ϕ_{31} and T_{31} in expansions (2.4) are inhomogeneous versions of those for ϕ_{11} and T_{11} with forcing terms given in terms of the linearized eigensolutions. These equations only have a solution if a solvability criterion is satisfied which fixes the value of R_2. This criterion is derived by the usual procedure of examining adjoint systems, although in the present case the linearized system is self-adjoint. This procedure is omitted for brevity but it leads to a Landau equation for the amplitude, A, whose steady supercritical value is given by

$$A^2 = \frac{8a^2 R_2}{(\pi^2 + a^2)^3}. \qquad (2.6)$$

The onset of convection is via a pitchfork bifurcation from the stable zero state when $R_2 < 0$ to a weakly convecting state when $R_2 > 0$.

In this paper we are interested in convection in a high aspect ratio container, and this corresponds to a large vortex wavenumber, $a \gg 1$. Further, it is necessary to impose boundary conditions on the sidewalls, which will be taken to be at $x = 0$ and $x = \pi/a$. For simplicity we shall assume that the boundaries are insulated and impermeable; cases where the sidewalls have a fixed, linearly decreasing temperature have recently been considered by Rees and Lage (**12**). Unlike the case of the Bénard problem in which no-slip conditions must be satisfied, the infinite layer analysis, as far as we have already expounded it, is immediately applicable to convection in a container with rectangular cross-section. Equation (2.6) shows that with $R_2 = O(1)$ then $A \sim O(a^{-2})$ as $a \to \infty$ and in this large wavenumber limit expansions (2.4) attain the forms

$$\psi = \varepsilon a^{-1} \hat{A} \sin \pi y \sin ax + \varepsilon^2 a^{-4} \hat{A}^2 \hat{\phi}_{22} \sin 2ax + ..., \qquad (2.7a)$$

$$\theta = 1 - y + \varepsilon \hat{A} a^{-2} \sin \pi y \cos ax + \varepsilon^2 \hat{A}^2 [(2\pi a^2)^{-1} \sin 2\pi y + \hat{T}_{22} \cos 2ax] + ..., \qquad (2.7b)$$

where we have written $\hat{A} = a^2 A$, $\hat{\phi}_{22} = a^3 \phi_{22}$ and $\hat{T}_{22} = a^4 T_{22}$ with the circumflex notation denoting $O(1)$ quantities. It is clear that because A becomes small in the $a \gg 1$ limit (see (2.6)), it is possible to relax the assumption that ε is small. A little experimentation reveals that in fact ε

can be as large as $O(1)$ without changing the essential structure of the analysis. With this size of ε, the perturbations to the temperature field remain asymptotically smaller than the basic conduction profile, but now the corrections to the mean temperature field and the first harmonic are the same size, namely $O(a^{-2})$ (notice that in (2.7b) $\hat{T}_{22} = 0$ from (2.5e)). Furthermore, the vertical velocity of the fluid is now $O(1)$—this can be seen by forming $v = \psi_x$ and allowing $a \to \infty$ with $\varepsilon = O(1)$. This regime therefore heralds a much stronger convection field which is examined in detail presently. For convenience, much of the notation introduced in this section will be reused in sections 3, 4, sometimes with altered meanings. Whilst this may seem somewhat perverse, each of the coming sections is more-or-less self-contained so no confusion should arise through the repeated use of notation and, in compensation, we are not forced to introduce a plethora of different symbols.

3. Intermediate-strength large wavenumber convection

The results described in section 2 indicate that for large wavenumbers there is a solution of (2.1), (2.2) with

$$\theta = 1 - y + a^{-2}\bar{\theta}_2 + a^{-2}(\theta_{10} + a^{-2}\theta_{12} + \ldots)\cos ax + a^{-8}\theta_{20}\cos 2ax + \ldots, \tag{3.1a}$$

$$u = a^{-1}(u_{10} + a^{-2}u_{12} + \ldots)\sin ax + a^{-7}u_{20}\sin 2ax + \ldots, \tag{3.1b}$$

$$v = (v_{10} + a^{-2}v_{12} + \ldots)\cos ax + a^{-6}v_{20}\cos 2ax + \ldots, \tag{3.1c}$$

$$p = a^2\bar{p}_0 + \bar{p}_2 + a^{-2}(p_{10} + a^{-2}p_{12} + \ldots)\cos ax + a^{-8}p_{20}\cos 2ax + \ldots, \tag{3.1d}$$

where

$$R = a^2 + R_2 + \ldots \quad \text{as} \quad a \to \infty \tag{3.1e}$$

and where $\bar{p}_{ij}$, θ_{ij} and v_{ij} are functions of y alone. It is worth remarking on the very small size of the second harmonic terms. The relevant scalings arise as a result of the findings of section 2 that in expansions (2.4) the harmonic terms ϕ_{22} and T_{22} vanish. Calculation of $O(\varepsilon^4)$ terms in (2.4) then reveals that in our intermediate-strength expansions (3.1) the second harmonic quantities vanish down to the orders of a indicated. It is the very small size of these terms which allows the subsequent analytical progress.

On substitution of expansions (3.1) into the governing equations (2.1) we find that the leading order vortex quantities satisfy

$$\frac{dv_{10}}{dy} + u_{10} = 0, \qquad v_{10} = \theta_{10} \qquad \text{and} \qquad u_{10} = p_{10}. \tag{3.2a, b, c}$$

The mean pressure field is determined by the leading order y-momentum equation (2.1c) to give

$$\frac{d\bar{p}_0}{dy} = (1-y), \qquad \frac{d\bar{p}_2}{dy} = R_2(1-y) + \bar{\theta}_2, \tag{3.3a, b}$$

whilst the leading order mean relations arising from the energy and x-momentum equations are automatically satisfied. The second order temperature term is derived from the mean flow components of the energy equation

$$\frac{d\bar{\theta}_2}{dy} = \tfrac{1}{2}\theta_{10}^2 - \overline{A}_2, \tag{3.4}$$

where $\overline{A}_2$ is the constant of integration which, on applying the boundary conditions $\bar{\theta}_2 = 0$ on $y = 0$ and $y = 1$, is given by

$$\overline{A}_2 = \tfrac{1}{2}\int_0^1 \theta_{10}^2 dy. \tag{3.5}$$

At next order the equations for the second order vortex terms v_{12} and u_{12} derived from (3.1) and (2.1) lead to a consistent solution only if

$$2\frac{d^2\theta_{10}}{dy^2} + R_2\theta_{10} - \tfrac{1}{2}\theta_{10}\left(\theta_{10}^2 - \int_0^1 \theta_{10}^2 dy\right) = 0 \tag{3.6a}$$

subject to

$$\theta_{10} = 0 \qquad \text{on} \qquad y = 0, 1. \tag{3.6b}$$

We note that (3.6a) may be rescaled to obtain the corresponding equation for the Bénard problem found in (**8**). This second order nonlinear equation shows that the correction to the mean flow $\bar{\theta}_2$ and the fundamental term θ_{10} are determined simultaneously rather than sequentially (cf. usual weakly nonlinear theory). Analytical solution of (3.6) is possible and if $E(m)$ and $K(m)$ denote the elliptic integrals of the first and second kind respectively then we can write θ_{10} parametrically as

$$N = \tfrac{1}{2}R_2 + \tfrac{1}{4}\int_0^1 \theta_{10}^2 dy, \qquad K(m) = \frac{1}{2}\left(\frac{N}{1+m}\right)^{\frac{1}{2}}, \tag{3.7a, b}$$

$$\theta_{10} = 2\left(\frac{2mN}{1+m}\right)^{\frac{1}{2}} \operatorname{sn}\left[\left(\frac{N}{1+m}\right)^{\frac{1}{3}} y \,\middle|\, m\right], \tag{3.7c}$$

$$\int_0^1 \theta_{10}^2 dy = \frac{32K(m)}{m}[K(m) - E(m)]. \tag{3.7d}$$

Equations of the form (3.6) have been previously derived by Knobloch and Proctor (**13**) and Proctor and Holyer (**14**) in the context of convection cells in double diffusive systems. Proctor and Holyer examined the planform selection mechanisms for tall thin modes and used two-scale methods to derive nonlinear evolution equations for interacting roll solutions. The parametric form of (3.7) admits multiple solutions and, for small amplitudes, these match directly onto the weakly nonlinear solutions of section 2. (The physically most important weakly nonlinear mode, in the sense that it occurs at the least value of R_N, is as given by (2.5). However, there is a sequence of higher modes in which T_{11} and ϕ_{11} are proportional to $\sin n\pi y$, $n = 2, 3, \ldots$.) When R_2 is large, the parameter m is very close to unity and the sn function in (3.7c) is then approximately constant away from the boundaries. Multiple solutions continue to exist in this limit but they differ from each other by only exponentially small quantities.

Although (3.7) is the formal solution of (3.6), it is not particularly illuminating and, for the range of values $2\pi^2 < R_2 < \infty$, system (3.6) can be easily solved using a standard fourth order Runge–Kutta numerical technique coupled to a multiple shooting code. The dependence of $\bar{A}_2$ on R_2 is shown in Fig. 1a and the structures of θ_{10} and $\bar{\theta}_2$ are illustrated in Figs 1b, c. For values of R_2 close to $2\pi^2$ an expansion of the form

$$R_2 = 2\pi^2 + r_2\delta + \ldots, \qquad \bar{A}_2 = a_2\delta + \ldots, \tag{3.8a, b}$$

$$\theta_{10} = \delta^{\frac{1}{2}}(B_{10} + \delta B_{12} + \ldots)\sin\pi y + \ldots, \qquad \bar{\theta}_2 = -(B_{10}^2\delta \sin 2\pi y)/8\pi + \ldots, \tag{3.8c, d}$$

gives $B_{10}^2 = 4a_2 = 8r_2$, which matches with the structure of the appropriate weakly nonlinear solution described in section 2. For large values of R_2 the numerical solutions show the emergence of the distinctive asymptotic state and it may be shown, using (3.4) to (3.6), that as $R_2 \to \infty$,

$$\bar{A}_2 \sim \tfrac{1}{16}R_2^2 - R_2 + \text{exponentially small terms}, \tag{3.9a}$$

and

$$\theta_{10} = \frac{R_2}{2\sqrt{2}}[\tanh \tfrac{1}{8}R_2 y + \tanh \tfrac{1}{8}R_2(1-y) - 1] + \text{exponentially small terms} \tag{3.9b}$$

is the appropriate composite solution of (3.6a) for $0 \leq y \leq 1$. Furthermore it is straightforward to show that

$$\bar{\theta}_2(y) \sim R_2(y-1) \tag{3.9c}$$

across the majority of $0 \leq y \leq 1$. However, as this solution does not satisfy the requisite conditions on the endwalls, boundary layers need to be introduced there. The asymptotic prediction (3.9a) is shown in Fig. 1a and is seen to be in excellent agreement with the numerical solution of (3.6a) once R_2 is greater than approximately 40.

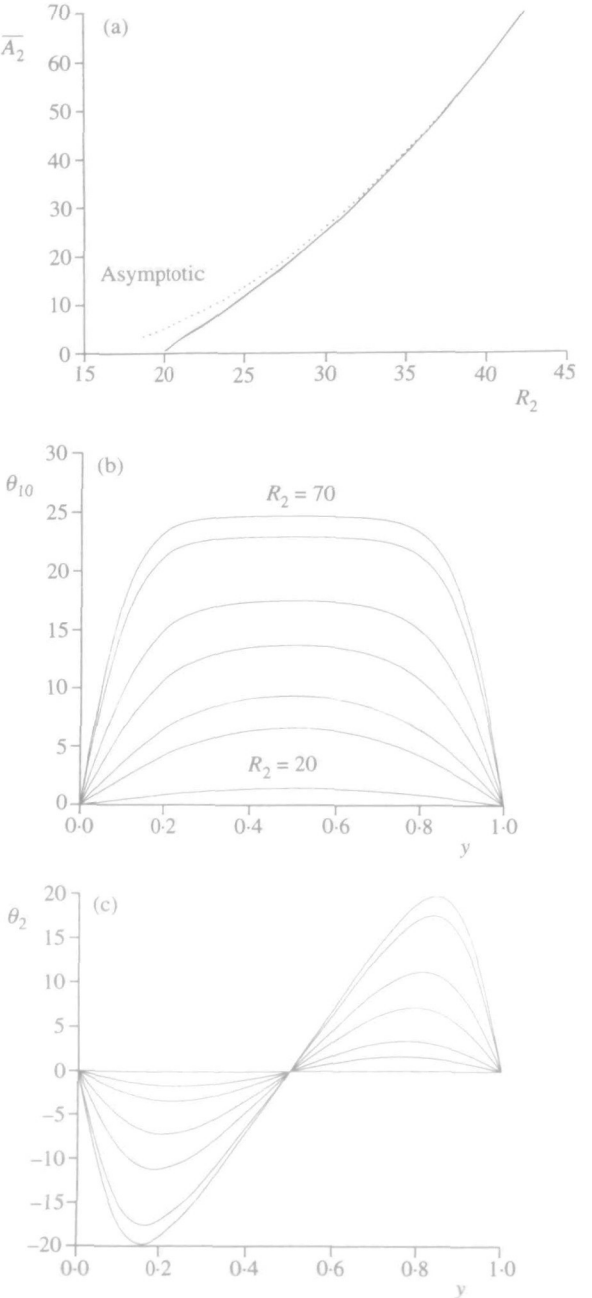

FIG. 1. (a) The dependence of $\overline{A}_2$ on the Darcy–Rayleigh number R_2. The dotted line denotes the large R_2 asymptotic prediction (3.9a). (b) The structure of the eigenfunction $\theta_{10}(y)$ corresponding to $R_2 = 20, 25, 30, 40, 50, 70$. (c) The form of the mean flow temperature term $\overline{\theta}_2(y)$ for the same choices of R_2 as used in (b)

The large R_2 results (3.9) and the numerical solutions confirm that the strength of the cellular motion increases with R_2. This numerical solution also demonstrates the formation of the expected boundary layers attached to $y = 0$ and $y = 1$. These layers are of thicknesses $O(R_2^{-1})$ and so, when $R_2 \sim a$, they are of depth comparable to the wavelength of the convection cells. Then we can expect that all the harmonics of the vortex disturbance will be of equal amplitudes inside the boundary zones which will thereby become fully nonlinear and only amenable to a numerical solution. It is this nonlinear structure which we describe in section 4.

4. Strongly nonlinear convection

The results described above indicate that when the Rayleigh number is $O(a)$ above the linear neutrally stable value the flow field develops a three-layer structure which comprises a central core supplemented by boundary layers at each endwall. Based on the analysis detailed above we anticipate expansions in the core of the forms

$$\theta = 1 - y + a^{-1}\bar{\theta}_1 + a^{-1}(\theta_{10} + a^{-1}\theta_{11} + \ldots)\cos ax + a^{-4}\theta_{20}\cos 2ax + \ldots, \tag{4.1a}$$

$$u = (u_{10} + a^{-1}u_{11} + \ldots)\sin ax + a^{-3}u_{20}\sin 2ax + \ldots, \tag{4.1b}$$

$$v = a(v_{10} + a^{-1}v_{11} + \ldots)\cos ax + a^{-2}v_{20}\cos 2ax + \ldots, \tag{4.1c}$$

$$p = a^2\bar{p}_0 + a\bar{p}_2 + a^{-1}(p_{10} + a^{-1}p_{11} + \ldots)\cos ax + a^{-4}p_{20}\cos 2ax + \ldots, \tag{4.1d}$$

with

$$R = a^2 + aR_1 + \ldots \tag{4.1e}$$

and where $\bar{p}_i$, θ_{ij}, u_{ij} etc. are functions of y only. The leading order vortex terms derived by substitution of (4.1) into (2.1) are given by

$$\frac{dv_{10}}{dy} + u_{10} = 0, \qquad v_{10} = \theta_{10} \qquad \text{and} \qquad u_{10} = p_{10}. \tag{4.2}$$

On considering the leading order mean terms in the energy equation we obtain an equation for $\bar{\theta}_{10}$ which can be integrated easily to give

$$\bar{\theta}_{10} = 2\gamma, \tag{4.3}$$

where γ is a constant of integration which measures the core cellular strength. The corresponding terms in the y-momentum equation lead to expressions for the mean flow pressure distribution but this is not required

here. The equations for the second order cellular terms, as in section 3, lead to the consistency condition

$$\frac{d\bar{\theta}_1}{dy} = R_1, \tag{4.4}$$

thereby giving the mean temperature distribution. It is obviously impossible to both solve (4.4) and simultaneously satisfy both temperature boundary conditions at the endwalls. We appeal to the numerical results of Fig. 1c and to the large R_2 asymptotic solution of (3.6), which together suggest that in the present strongly nonlinear convection the mean temperature correction is a function which is odd about $y = \frac{1}{2}$. Therefore we take

$$\bar{\theta}_1 = R_1(y - \tfrac{1}{2}) \tag{4.5}$$

and introduce boundary layers in order to fulfill boundary conditions (2.2). As in the nonlinear Bénard convection work of (**8**) and the nonlinear Görtler vortex study by Bassom and Blennerhassett (**15**) all the harmonics of the cellular motion are of comparable size within these $O(a^{-1})$ depth zones.

In the layer adjacent to $y = 0$ we define the $O(1)$ coordinates X, Y by

$$X = ax, \qquad Y = ay \tag{4.6}$$

and the flow quantities are expanded as

$$u = aU(X, Y) + ..., \qquad v = aV(X, Y) + ..., \tag{4.7a, b}$$

$$p = \text{constant} + aY + P(X, Y) + ..., \qquad \theta = 1 + a^{-1}T(X, Y) + ... \tag{4.7c, d}$$

Substitution of (4.7) into (2.1) yields boundary layer equations of the form

$$U_X + V_Y = 0, \tag{4.8a}$$

$$U = -P_X, \tag{4.8b}$$

$$V = -P_Y + T + R_1, \tag{4.8c}$$

$$UT_X + VT_Y = T_{XX} + T_{YY}, \tag{4.8d}$$

which must be solved subject to the conditions

$$V = 0, \qquad T = 0 \qquad \text{on} \qquad Y = 0 \tag{4.8e, f}$$

along with the matching conditions

$$V \to 2\gamma \cos X, \quad U \to 0, \quad T \to -Y - \tfrac{1}{2}R_1 + 2\gamma \cos X \quad \text{as} \quad Y \to \infty. \tag{4.8g, h, i}$$

The system of equations (4.8) constitutes a nonlinear eigenvalue problem for γ as a function of the scaled Rayleigh number parameter R_1.

4.1 *Numerical solution of the boundary layer equations*

In order to obtain numerical solutions of (4.8) it is convenient to use a streamfunction formulation for the equations. Thus we define

$$V = \Psi_X, \qquad U = -\Psi_Y, \tag{4.9}$$

and hence system (4.8) can be rewritten as

$$\Psi_{XX} + \Psi_{YY} = T_X, \tag{4.10a}$$

$$\Psi_X T_Y - \Psi_Y T_X = T_{XX} + T_{YY}. \tag{4.10b}$$

The symmetries inherent to the equations and boundary conditions imply that T and Ψ may be expressed as Fourier cosine and sine series in X respectively. Therefore we look for solutions of the form

$$T = \sum_{j=0}^{N} T_j(Y)\cos jX, \qquad \Psi = \sum_{j=1}^{N} V_j(Y)\sin jX, \tag{4.11a, b}$$

where the Fourier series have necessarily been truncated after a finite number of modes N. The expansions (4.11) reduce equations (4.10) to a boundary value problem consisting of $2N+1$ coupled, nonlinear second order differential equations with γ as an eigenvalue. The specification of the problem is completed by the constraints

$$T_0 = 0, \qquad T_j = V_j = 0 \qquad 1 \le j \le N, \tag{4.12a}$$

on the endwall $Y = 0$ together with matching conditions with the core solution (4.5)

$$T_0 \to -Y - \tfrac{1}{2}R_1, \qquad T_1 \to \gamma, \qquad V_1 \to \gamma \qquad \text{as} \qquad Y \to \infty. \tag{4.12b}$$

It should be noted at this stage that the appropriate boundary layer equations in the thin zone attached to the other endwall at $y = 1$ can be easily scaled to take the form of (4.9) to (4.12). Thus the symmetry in the configuration assures us that we only need to solve one set of boundary layer equations.

The results presented here were obtained using a numerical procedure closely allied to the Keller-box method. This method is very frequently used to solve non-similar boundary layer flows in which the flow profiles vary with the streamwise coordinate. In such marching problems the governing equations are usually reduced to first order form in the cross-stream coordinate and then approximated using central differences with the resulting difference equations solved using Newton–Raphson iteration. The Keller-box method is one which has been applied to a very wide variety of problems and the particular implementation which is used as the basic solver is one where a numerical differentiation procedure is used to generate the Jacobian iteration matrix rather than having to specify it explicitly (Rees and Pop (**16**), Rees and Bassom (**17**)). The numerical implementation used for the

present problem involved two fundamental adaptations of the basic Keller-box philosophy. First, the equations solved were not reduced to first order form, but were left in second order form; this has the advantage of leading to an increased numerical conditioning of the Jacobian matrix. Second, the code was extended to include a procedure for computing eigenvalues. The resulting Jacobian matrix is no longer block-tridiagonal for it is supplemented by an extra column and row of matrix blocks. The block tridiagonal matrix algorithm was then adapted to allow for the modified configuration and the entries were themselves computed numerically in preference to explicit specification within the code. For the present calculation the 'streamwise coordinate' used in the basic Keller-box method was replaced by the parameter R_1, and therefore the structure of the program easily enabled us to perform a parameter sweep through a range of values of R_1. In practice we found it sufficient to truncate the computational domain at $Y = Y_\infty = 40$ and to take $N = 11$ as the upper limit in the Fourier sums (4.11). Other values of N and Y_∞ were also used in order to verify convergence of results. Taking $N = 11$ was found to be adequate for values of the Rayleigh parameter R_1 up to about 200; beyond this value more modes are needed to give the required resolution in the X–direction. Our computations described here were based on $R_1 \leqslant 200$ although the adjustments required in order to derive reliable results for higher R_1 are quite straightforward to implement.

Figure 2 shows streamfunction plots corresponding to progressively larger values of R_1. In each subfigure the fluid is moving down the $X = 0$ sidewall and turning at the $Y = 0$ endwall before returning to the core. When R_1 is sufficiently small the solution is virtually symmetric about $X = \frac{1}{2}\pi$ and the numerical solution is predominantly confined to the zeroth and first terms in (4.11); thus the solution of the last section is recovered in this $R_1 \to 0$ limit. As R_1 increases the solution loses its symmetry and the region within which the fluid turns near $Y = 0$ becomes smaller. The fluid motion becomes particularly intense near the $Y = 0$, $X = \pi$ corner.

Figure 3 shows the mean temperature profile, $T_0(Y)$, for a variety of values of R_1. All slopes shown in Fig. 3 asymptote to -1 when Y is sufficiently large, but the solutions near $Y = 0$ are of interest. Near $Y = 0$ the slope of the mean temperature profile becomes increasingly negative as R_1 increases. When R_1 is sufficiently large the profile has a minimum value near to $Y = 1$. We note that this behaviour is qualitatively different from the results presented by Blennerhassett and Bassom (**8**) who found that the mean flow component $T_0(Y)$ in strongly nonlinear Bénard convection appears to develop a large region of near constant temperature before attaining the large-Y linear part of the solution. No evidence of a corresponding feature is observed here.

Figure 4 shows the variation of the parameter γ with R_1. Also shown are the large R_1 solution with $N = 1$ obtained in section 4.2 below and the numerical solution of system (4.10) when $N = 1$ in the Fourier sums (4.11).

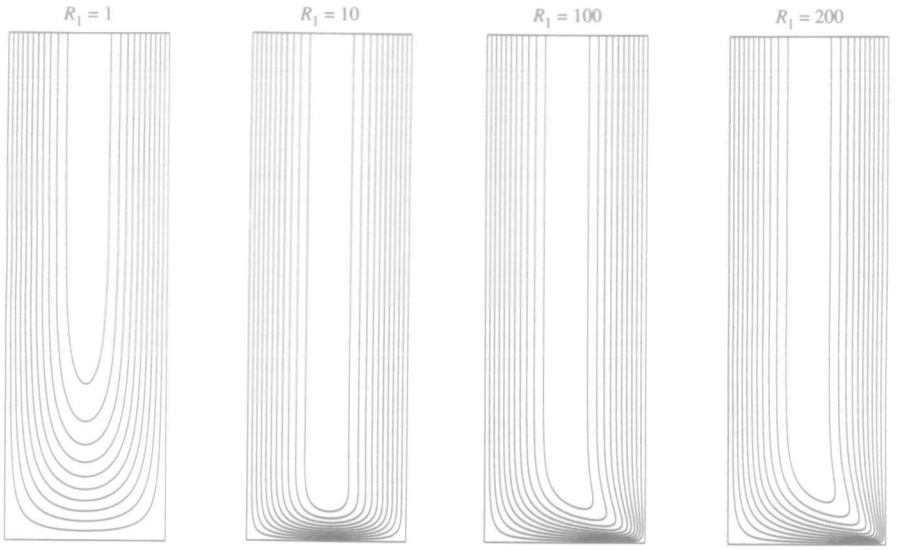

FIG. 2. The lines of constant Ψ for the solution of equations (4.8) when the Fourier sums (4.11) are truncated with $N = 11$. In each case the domain shown is $0 \leq X \leq \pi$, $0 \leq Y \leq 40$ and the four plots correspond to R_1 given by (a) 1, (b) 10, (c) 100, (d) 200. The interval $\Delta\Psi$ between successive contours and the maximum values Ψ_{max} in each of the four cases is (a) $\Delta\Psi = 0{\cdot}032$, $\Psi_{max} = 0{\cdot}321$; (b) $\Delta\Psi = 0{\cdot}278$, $\Psi_{max} = 2{\cdot}774$; (c) $\Delta\Psi = 1{\cdot}303$, $\Psi_{max} = 13{\cdot}032$; (d) $\Delta\Psi = 1{\cdot}949$, $\Psi_{max} = 19{\cdot}486$

For this single harmonic truncation of (4.8) there is an offset between the numerical and asymptotic results. The reason for this is that the asymptotic prediction derived in section 4.2 only considers the leading order behaviour and the ratio between successive terms in the expression for R_1 when $\gamma \gg 1$ decays only very slowly. Thus we can only expect a good agreement between numerical and asymptotic predictions at extremely large values of γ (far greater than those considered here). However, the fact that the two methods give qualitatively similar results based on only one term in the asymptotic expansion means that we can have confidence in results arising from our numerical code.

4.2 *Asymptotic solution of the boundary layer equations as* $R_1 \to \infty$

We have seen that an asymptotic analysis shows that only the mean and fundamental modes of the vortex play a role in determining the core flow. As an approximation this structure is imposed in the boundary layer as γ gets large. This can be regarded as the single harmonic version of the equations solved numerically in section 4.1 and provides some analytical results against

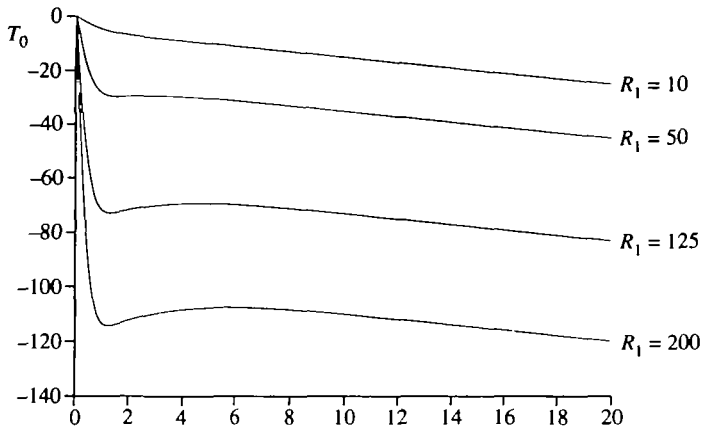

FIG. 3. The mean temperature profiles corresponding to (a) $R_1 = 10$; (b) $R_1 = 50$; (c) $R_1 = 125$; (d) $R_1 = 200$

which the numerical results described above may be compared. The requisite equations are

$$V_1'' - V_1 = -T_1 \qquad \text{and} \qquad T_1'' - (2V_1^2 + 1)T_1 = -(2\gamma^2 + 1)V_1 \quad (4.13a, b)$$

with the mean temperature term T_0 given by the integration of

$$T_0' = 2(T_1 V_1 - \gamma^2) - 1. \quad (4.13c)$$

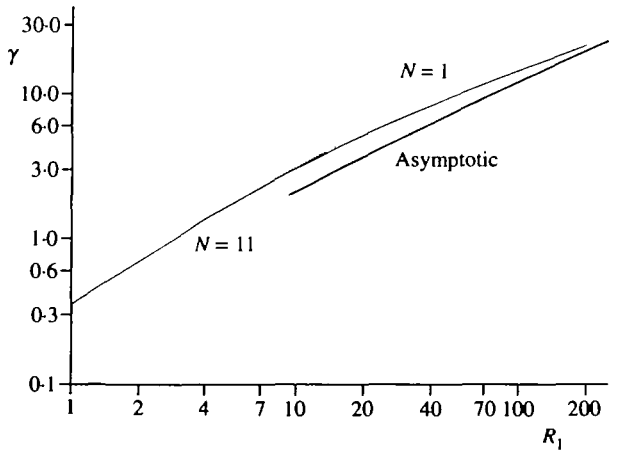

FIG. 4. The variation of γ with R_1. The thin solid line denotes the results obtained using truncation at 11 harmonics whilst the dotted line denotes the results using only one harmonic. Finally, the thick solid line shows the form of the one term asymptotic prediction (4.23) which is valid for $\gamma \gg 1$

Equations (4.13) must be solved subject to the boundary conditions

$$T_0 = T_1 = V_1 = 0 \qquad \text{at} \qquad Y = 0 \tag{4.14a}$$

along with the matching conditions

$$V_1, T_1 \to \gamma, \qquad T_0 \to -Y - \tfrac{1}{2}R_1 \qquad \text{as} \qquad Y \to \infty. \tag{4.14b}$$

In the region where $Y = O(1)$ we start from the hypothesis that

$$T_1 = \gamma T_{10}(Y) + O(\gamma^{-1}) + ..., \qquad V_1 = \gamma V_{10}(Y) + ... \tag{4.15a, b}$$

which, on substitution into (4.13a,b), yield

$$T_{10}V_{10} = 1, \qquad V_{10}'' - V_{10} = -\frac{1}{V_{10}}. \tag{4.16a, b}$$

After multiplication by V_{10}' equation (4.16b) can be integrated to give

$$\left(\frac{dV_{10}}{dY}\right)^2 = V_{10}^2 - 2\ln V_{10} - 1, \tag{4.17}$$

where the constant of integration has been determined by insisting that $V_{10} \to 1$ as $Y \to \infty$.

An analysis of (4.17) in the limit $Y \to 0$ demonstrates that

$$V_{10} \to \sqrt{2}Y\sqrt{-\ln Y} + ... \tag{4.18}$$

and the expression for T_{10} given by (4.16a) indicates the existence of a viscous region of depth $\delta = O(\gamma^{-\frac{1}{2}}(\ln\gamma)^{-\frac{1}{4}})$. Here we define

$$Y = \gamma^{-\frac{1}{2}}(\ln\gamma)^{-\frac{1}{4}}\hat{Y} \tag{4.19}$$

with $\hat{Y} \sim O(1)$, and we write

$$T_1 = \gamma\delta^{-1}(-\ln\delta)^{-\frac{1}{2}}\hat{T} + ..., \qquad V_1 = \gamma\delta(-\ln\delta)^{\frac{1}{2}}\hat{V} + ... \tag{4.20a, b}$$

Conditions (4.14a) and (4.14b) require that $\hat{V} = \hat{T} = 0$ at $Y = 0$ and $\hat{V} \to \sqrt{2}\hat{Y}$, $\hat{T} \to (\sqrt{2}\hat{Y})^{-1}$ as $Y \to \infty$. On substitution of (4.20) into (4.13) it is then straightforward to show that

$$\hat{V} = \sqrt{2}\hat{Y}, \qquad \frac{d^2\hat{T}}{d\hat{Y}^2} - 4\hat{Y}^2\hat{T} = -2\sqrt{2}\hat{Y}, \qquad \frac{d\hat{T}_0}{d\hat{Y}} = 2(\hat{V}\hat{T} - 1). \tag{4.21a, b, c}$$

If we now define $\hat{T} = 2^{-\frac{1}{4}}T^*$ and $\hat{Y} = 2^{-\frac{1}{4}}Y^*$ then equation (4.21b) can be written

$$\frac{d^2T^*}{d(Y^*)^2} - 2(Y^*)^2T^* = -2Y^*, \tag{4.22}$$

and is subject to $T^* = 0$ on $Y^* = 0$ and $T^* \to (1/Y^*)$ as $Y^* \to \infty$.

It follows from the boundary conditions (4.14b) together with (4.13c) and (4.20) to (4.22) that

$$R_1 = -2^{7/4}\delta\gamma^2 \int_0^\infty (Y^*T^* - 1)\,dY^* + \ldots = 3{\cdot}00\gamma^{3/2}(\ln\gamma)^{-1/4} + \ldots \qquad (4.23)$$

and the comparison between this asymptote and the corresponding numerical solution using only one harmonic is shown in Fig. 4.

5. Discussion

In this work we have examined the structure of steady strongly nonlinear vortices in a saturated porous medium within a tall, large aspect ratio vertical container. The main result we have is that the previously found strongly nonlinear modes in Görtler flow and Bénard convection have a direct counterpart in this porous medium configuration. However, there is a crucial difference between our work here and some of the other studies which may well have implications concerning the possible physical importance of the modes. In the Görtler analysis, it is found that for large vortex wavenumber a the linear neutral Görtler number G_N is $O(a^4)$ and fully nonlinear modes can only arise once the Görtler number (which plays a role akin to that of the Rayleigh number here) satisfies $(G - G_N)/G_N = O(1)$. For the Bénard problem discussed in (**8**), strongly nonlinear vortices appear once $(R - R_N)/R_N = O(a^{-1})$, where R_N is the linear neutral Rayleigh number. As $R_N = O(a^4)$ the nonlinear domain is approached at parameter values $O(a^3)$ above the linear neutral stability curve. This should be contrasted with the present formulation in section 4. Equation (4.1e) indicates that strongly nonlinear motions are possible at distances only $O(a)$ above linear neutrality. Thus the nonlinear vortices discussed in this paper occur quite close to the neutral curve and it is therefore plausible that they are of significant practical importance. It must be recalled, however, that we are strictly only entitled to draw this conclusion for modes within a box whose horizontal dimensions are much shorter than its height. In cases where this length disparity is absent we cannot legitimately appeal to our strongly nonlinear analysis for the preferred modes will not be of short wavelength and a proper description of the flow requires direct computations using the full equations.

Fully nonlinear vortices in the tall container acquire the distinctive core-boundary layer structure. The vortices in the central core can be deduced by solving simple consistency conditions which reflect the fact that the mean flow and first harmonic component are closely coupled together. The boundary layers are necessary in order to ensure that the core solutions are modified appropriately so as to satisfy the imposed conditions on the endwalls of the container. These boundary layers necessitate a numerical solution which suggests that a well-defined vortex configuration must evolve as the intensity of the modes increases yet further. This next stage of nonlinearity has yet to be identified in either the present porous medium

problem or the study of (8). In order to describe this stage it is necessary to ascertain the formal asymptotic solution of (4.10) to (4.12) in the large-γ limit and preliminary studies suggest that this is a formidable task.

Lastly, it must be remembered that here we have concentrated on steady vortices. It might be argued that time-dependent modes cannot be ignored and, of course, for a complete description of the problem this should be considered. However, we note that the standard weakly nonlinear analysis summarized in section 2 shows that our flow is supercritically stable: that is, according to usual Stuart–Landau theory it evolves to a stable finite amplitude steady state. Naturally, we cannot therefore definitely conclude that our highly nonlinear steady motions *must* constitute the preferred mode but it would not be surprising if this turned out to be the case. A completely nonlinear unsteady computation is beyond the scope of the present work but a natural extension of our study would be an investigation into the possibility of any time-dependent modes.

Acknowledgements

We thank the referees for their useful comments on this paper. The first author is grateful to the EPSRC for financial support whilst this work was carried out.

REFERENCES

1. C. L. TIEN and K. VAFAI, *Adv. appl. Mech.* **27** (1990) 225–281.
2. D. A. NIELD and A. BEJAN, *Convection in Porous Media* (Springer, Berlin 1992).
3. D. A. S. REES, *J. theor. appl. Mech.* to appear.
4. J. T. STUART, *J. Fluid Mech.* **9** (1960) 353–370.
5. J. WATSON, *ibid.* **9** (1960) 371–389.
6. E. PALM, J. E. WEBER and O. KVERNVOLD, *ibid.* **54** (1972) 153–161.
7. P. HALL and W. D. LAKIN, *Proc. R. Soc.* A **415** (1988) 421–444.
8. P. J. BLENNERHASSETT and A. P. BASSOM, *IMA J. appl. Maths* **52** (1994) 51–77.
9. A. P. BASSOM and K. ZHANG, *Geophys. Astrophys. Fluid Dynamics* **76** (1994) 223–238.
10. D. A. S. REES and D. S. RILEY, *Proc. R. Soc.* A **421** (1989) 303–339.
11. —— and ——, *J. Fluid Mech.* **199** (1989) 133–154.
12. —— and J. L. LAGE, *Int. J. Heat Mass Transfer* **40** (1997) 111–121.
13. E. KNOBLOCH and M. R. E. PROCTOR, *J. Fluid Mech.* **108** (1981) 291–316.
14. M. R. E. PROCTOR and J. Y. HOLYER, *ibid.* **168** (1986) 241–253.
15. A. P. BASSOM and P. J. BLENNERHASSETT, *Proc. R. Soc.* A **439** (1992) 317–336.
16. D. A. S. REES and I. POP, *Trans. porous Media* **20** (1995) 223–234.
17. —— and A. P. BASSOM, *Int. J. Engng. Sci.* **34** (1996) 113–124.